ADVANCED OPTICAL MATERIALS
www.advopticalmat.de

WO_3-Based Electrochromic Distributed Bragg Reflector: Toward Electrically Tunable Microcavity Luminescent Device

Lili Xiao, Ying Lv, Jie Lin, Yongsheng Hu, Wenjie Dong, Xiaoyang Guo, Yi Fan, Nan Zhang, Jialong Zhao, Yunjun Wang, and Xingyuan Liu**

The electroresponsive WO_3-based electrochromic distributed Bragg reflectors (ECDBRs) are fabricated by means of one-step, room temperature glancing-angle electron-beam evaporation. The reflectance and Bragg wavelength of ECDBRs can be precisely and reversibly tailored on a large scale by simply applying a small bias voltage (±1.1 V) due to the electrochromic effect of the WO_3 layer, and this unique character is utilized to construct an electrically tunable microcavity luminescent device with embedded green CdSe@ZnS quantum dots (QDs). Therefore, large and reversible modulation in terms of photoluminescence (PL) peak intensity (18–335%), PL peak position (from 510.3 to 525.8 nm), and full width at half maximum (from 21.8 to 11.4 nm) from QDs in microcavity are achieved under electrical stimulus. The results will potentially provide a straightforward voltage-control route toward broadband tunable microcavity electroluminescent and lasing devices.

1. Introduction

Periodically structured materials with dimensions proportional to visible wavelength can modulate the flow of light and allow the creation of devices with additional photonic functionalities and/or improved performances.[1–3] Distributed Bragg reflectors (DBRs) in the form of periodic multilayer dielectric stacks with various refractive indices are critical components in optical feedback systems for lasers[4] and also play an important role in high-performance light-emitting devices,[5,6] photodetectors,[7] and solar cells.[8,9] The optical properties of such systems can be precisely tailored by manipulating the chemical composition and architecture (thickness and porosity) of stacked layers. Recently, special research interests lie in responsive DBRs, in which dynamical changes of the optical properties (reflectivity, band-gap, structural color) in response to external stimuli (such as light, temperature, chemical species, and electrical field) have been demonstrated.[10–13] Among them, electrical field is the most easily controlled stimulus and simplifies integration into existing electronic components, finding new applications in active filters, tunable laser sources, and color manipulation for optical communication and display technologies.

In this regard, redox-active polymers,[14–16] polyelectrolyte hydrogels,[17,18] liquid crystals,[19,20] or electrochromic materials[21,22] have been introduced into the periodic structure for realizing electrically tuned optical coatings. The shape and size manipulation using redox-active polymers, polyelectrolyte hydrogel, and liquid crystal usually cause large reflectance shifts, but slow response and poor durability, unsuitable for practical applications. By comparison, electrochromic materials can reversibly change their electronic structure and optical property (transmittance, reflectance, or absorption) under a small driving voltage and have been widely applied in energy-saving smart windows, switchable mirrors, and displays.[23–26] This color change is mainly caused by the adjustable absorption as well as change of refractive index. Moreover, electrochormic materials have unique open-circuit memory effect (bistability in colored and bleached states), making it possible to prepare devices with low energy consumption and good stability.[27] DBRs employ two kinds of electrochromic materials with different refractive indices such as WO_3 and NiO and have shown electrically tunable reflectivity and photonic stop-band.[22] However, the preparation process was relatively complex with the requirement for high-temperature calcination at 450 C after depositing of each layer. In addition, complementary coloration effects of WO_3 (cathodic coloration) and NiO (anodic coloration)

Dr. L. Xiao, Dr. Y. Lv, Dr. J. Lin, Dr. Y. Hu, W. Dong, Dr. X. Guo, Dr. Y. Fan, Dr. N. Zhang, Prof. J. Zhao, Dr. Y. Wang, Prof. X. Liu
State Key Laboratory of Luminescence and Applications
Changchun Institute of Optics
Fine Mechanics and Physics
Chinese Academy of Sciences
Changchun 130033, China
E-mail: lvying@ciomp.ac.cn; liuxy@ciomp.ac.cn
Dr. L. Xiao, Dr. W. Dong
University of Chinese Academy of Sciences
Beijing 100049, China
Prof. J. Zhao
Key Laboratory of Functional Materials Physics and Chemistry
of the Ministry of Education
Jilin Normal University
Siping 136000, China
Dr. Y. Wang
Suzhou Xingshuo Nanotech Co., Ltd. (Mesolight)
Suzhou 215123, China
The ORCID identification number(s) for the author(s) of this article can be found under https://doi.org/10.1002/adom.201700791.

DOI: 10.1002/adom.201700791

result in small reflectance modulation. Therefore, the development of responsive DBRs and DBR-based optical active devices with wide wavelength tuning capability using a modest and straightforward method are still highly desired.

In this study, the electroresponsive electrochromic DBRs (ECDBRs) based on monomaterial were constructed by an alternate depositing WO_3 layer with various porosities (refractive indices) using one-step glancing angle deposition (GLAD) combined with the electron-beam evaporation method at room temperature. By simply changing deposition angle and the thickness of each layer, the Bragg wavelength of ECDBRs can be continuously adjusted in visible light range. Most importantly, for each obtained ECDBR, the large and reversible modulations of Bragg wavelength and reflectance were achieved by simply applying a low driving voltage (±1.1 V) due to the bleaching or coloration of WO_3. Furthermore, taking a quantum dot (QD) luminescent material as an example, the ECDBRs were used to construct a tunable microcavity luminescent device for the first time. Large fluorescence (intensity, peak, and bandwidth) switching with clear cavity effects and good reversibility was realized under the control of applied voltage. The results demonstrate a simple way to achieve electroresponsive photonic crystals and have an instructive guidance for realizing active optical devices.

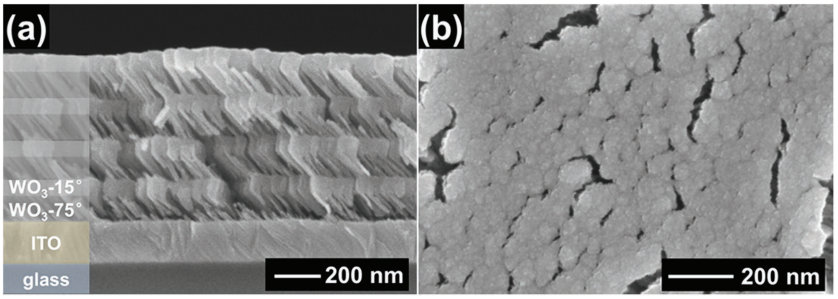

Figure 1. Cross-section and surface SEM images of a typical 4-bilayer ECDBR with a Bragg wavelength of 450 nm.

2. Results and Discussion

The ECDBRs were fabricated by alternately changing the deposition angle with the GLAD electron-beam deposition method. We have shown in our previous study that the porosity and refractive index of WO_3 films can be finely adjusted by changing the deposition angle between substrate and evaporation source.[28] The refractive index of the WO_3 films at 550 nm decreased from 1.94 to 1.56 with an increase of porosity from ≈15% to 58% as the grazing angle increased from 0° to 75°. In consideration of the index difference and deposition time together, the WO_3 films deposited at 15° and 75° (hereafter abbreviated as WO_3-15° and WO_3-75°) were employed as the high- and low-index layers, respectively, to construct ECDBRs. A continuous, smooth, and compact morphology was observed for WO_3-15° film, compared with oblique, ordered, and individual nanocolumn with large porosity for WO_3-75° film. The significant difference in the microstructures of both films results in a large index contrast of about 0.41 at 550 nm (1.97 vs 1.56), as shown in Figure S1 in the Supporting Information, which is larger than that for dense and porous WO_3 layers obtained by controlling the deposition pressure in radio frequency magnetron sputtering and enables us to construct a highly reflective mirror with less stacked layers, as discussed below.[29] **Figure 1** shows the SEM images of a representative 4-bilayer ECDBR, illustrating a clear and uniform interface without visible cracks and imperfections. The thickness of the low- and high-index layers are about 62 and 56 nm, respevtively, which are equivalent to quarter wavelength of the designed wavelength (450 nm). The microstructures of each layer in ECDBRs are similar to that of single WO_3 flm on indium tin oxide (ITO).[28] The WO_3-75° layer has a tilt and disjunctive nanocolumnar structure with a slant angle of ≈50°, a feature size less than 20 nm and pore diameter less than 15 nm. On the other hand, the WO_3-15° layer displays a close-grained morphology with some pores on the surface, which might be induced by the coarse grain surface of the underneath WO_3-75° layer. The alternative deposition of WO_3-75° and WO_3-15° films with different refractive indices satisfies the optical structure requirement for DBRs as well as the porous structure requirement for fast electrochemical reaction.

The peak position of the reflectance spectrum (Bragg wavelength, λ_B), the maximum reflectivity (R), and the bandwidth ($\triangle E$) (expressed in energy terms) are three important characteristic parameters of DBRs and can be expressed by the following equations[30,31]

$$m\lambda_B = 2\left(n_L h_L + n_H h_H\right) \tag{1}$$

$$R(N) = \left[\frac{n_0 - n_s\left(\frac{n_H}{n_L}\right)^{2N}}{n_0 + n_s\left(\frac{n_H}{n_L}\right)^{2N}}\right]^2 \tag{2}$$

$$\Delta E = \frac{4}{\pi} E \frac{|n_H - n_L|}{n_H + n_L}, \quad E = \frac{\hbar c}{\lambda_B} = \frac{1240}{\lambda_B}(\text{eV}) \tag{3}$$

where m is the order, n_H and n_L denote the refractive indices of high- and low-index layers, and h_H and h_L are the respective physical thicknesses. N is the number of bilayers, n_0 and n_s are the refractive indices of the incident and emergent medium (substrate), respectively.

Accordingly, by carefully adjusting the optical thickness of the WO_3-75° and WO_3-15° films (quarter-wave thickness), the reflecting dissimilar regions can be tailored with remarkable accuracy. **Figure 2**a,b shows the measured transmittance and reflectance spectra of three designed 4-bilayer ECDBRs with various film thicknesses. In contrast to the high visible-light transmittance of single WO_3-75° and WO_3-15° films on ITO (Figure S2, Supporting Information), the ECDBRs present well-defined and intense Bragg reflection through the whole visible light region. The Bragg peaks are located at about 450, 550, and 650 nm (abbreviated as ECDBR-450, ECDBR-550, and ECDBR-650, respectively, for convenience). An increase in the

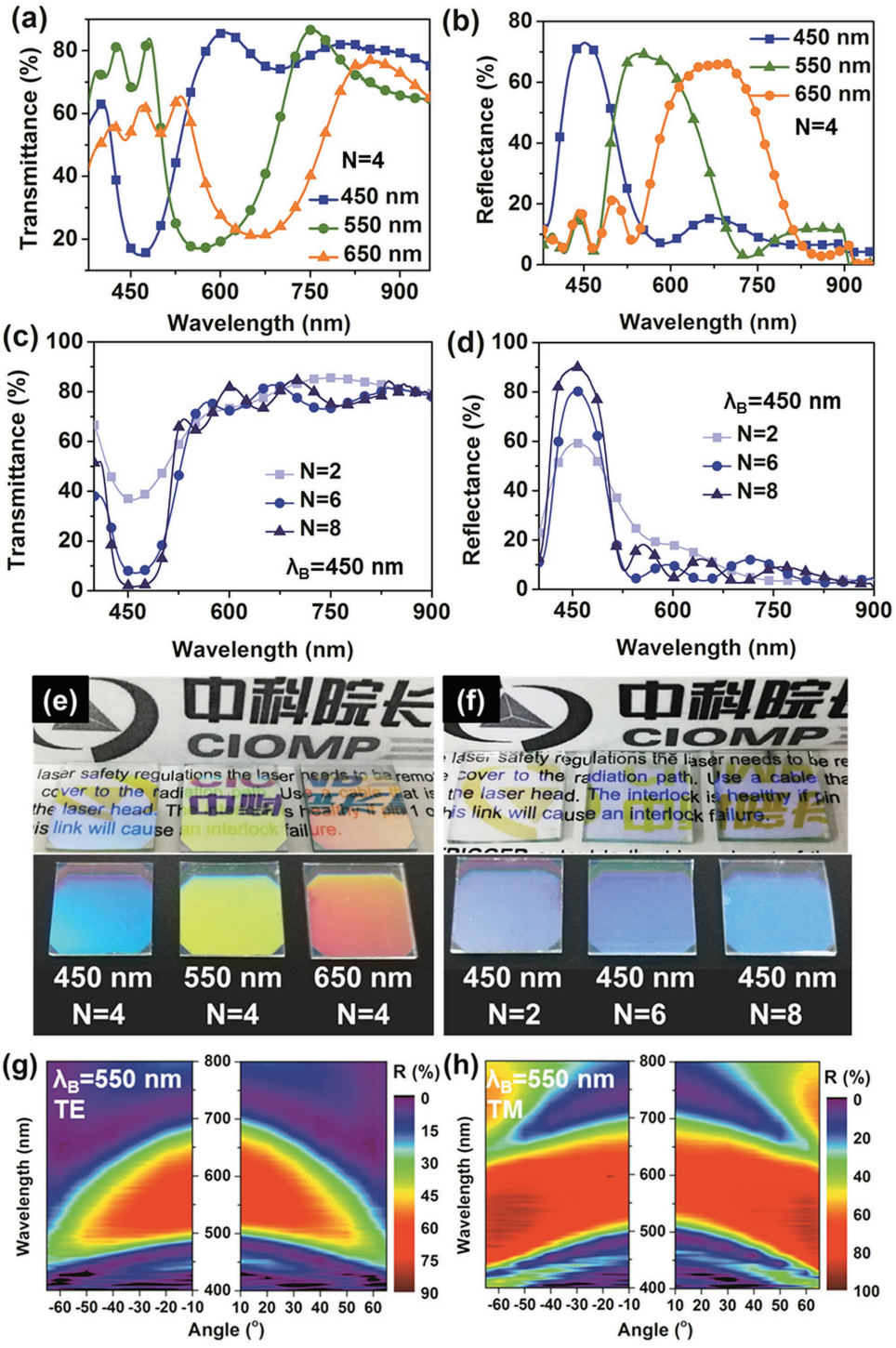

Figure 2. a,b) Transmittance and reflectance spectra at normal incidence of 4-bilayer ECDBR-450, ECDBR-550 and ECDBR-650, c,d) transmittance and reflectance spectra at normal incidence of 2-, 6-, and 8-bilayer ECDBR-450, e) photographs of 4-bilayer ECDBR-450, ECDBR-550 and ECDBR-650 from different viewing angles, f) photographs of 2-, 6-, and 8-bilayer ECDBR-450 from different viewing angles, experimental reflectance properties of 4-bilayer ECDBR-550 as a function of the incidence angle for g) s-polarized (TE) and h) p-polarized (TM) light.

physical thickness of each layer leads to a shift in the Bragg wavelength to lower energies typical with a slight increase in bandwidth (in the form of wavelength) and decrease in peak reflectivity, which is well consistent with the simulated results (Figure S3, Supporting Information). The decrease in peak reflectivity can be attributed to the reduction of refractive index contrast between WO_3-15° and WO_3-75° layers at long wavelength, as shown in Figure S1 in the Supporting

Information. The bandwidths of ECDBR-450, ECDBR-550, and ECDBR-650 are 91.2, 131.9, and 149.6 nm, respectively. According to Equation (3), the bandwidth can be tuned by Bragg wavelength and the refractive indices of WO_3-75° and WO_3-15°. In the cases of these three ECDBRs, the variation of Bragg wavelength (100 nm) is much bigger than that of n_L/n_H; thus, the bandwidth increases slightly along with the Bragg wavelength. Moreover, the almost antisymmetric spectral curves of reflectance and transmittance spectra implied that the absorption and scattering loss of these ECDBRs was very small (<10%). It is worth noting that benefited from the large index contrast (0.41 at 550 nm), the reflectance maxima of around 70% can be realized with only a 4-bilayer film. By comparison, other DBRs with monomaterial, prepared by radio frequency magnetron sputtering or anodization, have shown reflectivity of almost 80% with 27 or 60 alternate layers due to their small refractive index contrast.[29,32]

To study the thickness control and interfacial roughness properties, the atomic force microscopy (AFM) images of single WO_3-15° and WO_3-75° layers and 4-bilayer ECDBR-550, as well as SEM images of the ECDBR-550 over different positions have been measured (Figure S4, Supporting Information). The roughness of single WO_3 layer is similar in different position and the root mean square (RMS) values are between 3.6 and 3.9 nm. However, the average surface roughness of 4-bilayer ECDBR-550 increased to 14.96 ± 0.49 nm, which is well consistent with the SEM results. We simulate the effect of the roughness on reflectance of ECDBR-550 by sharing the undulate ($\triangle$ = 1.87 nm) on each layer (Figure S5, Supporting Information). It can be seen that such a surface roughness leads to a 9 nm difference of Bragg wavelength and 0.8% difference of peak reflectance, thus potentially causing some broadening of reflectance spectra. Besides the roughness, we also simulate the effect of bilayer number (N) on reflectance. When the N increases to 8, approximate "squared" reflectance spectrum is appeared. It follows that the shape of reflectance spectrum is affected by both roughness and N.

The reflectance maximum of ECDBRs can also be altered by controlling the number of layers in the stack. As expected, more intense reflectance was achieved by increasing the number of layers. The 4-(Figure 2b), 2-, and 6-bilayer (Figure 2d) ECDBR-450 show reflectance maximum of 73%, 60%, and 80%, respectively. The reflectivity of ECDBR can be even larger than 90% if we further increase the number of bilayers to 8 (Figure 2d). The good agreement between designed and experimental results strongly indicates that the GLAD method has good control over the growth of each layer. In addition, from the cross-section SEM image of the 8-bilayer ECDBR, we can see that the film structure does not collapse or deform as the number of layers increases (Figure S6, Supporting Information), denoting the feasibility of architecting ECDBRs with high reflectivity based on single WO_3 material using this method. The changes in reflectance can also be visually assessed. Figure 2e–f shows a series of pictures taken with a digital camera, in which ECDBRs with various thicknesses and number of layers display colorful optical characteristics, including brightly colored reflections and diversely perspective effects depending on the observation angle. To understand this angular-dependent optical property, the polarized reflectance properties of 4-bilayer ECDBR-550 on various incident angles are studied (Figure 2g–h). The symmetrical trend of the spectra for positive and negative angles illustrates that the orientation of microstructure has negligible effect on the reflectance spectrum. The reflectance peak for both s- and p-polarized light shifts toward higher energy with increasing the detection angles. When the incidence angles increased to 65°, a 98 nm blue-shift of reflectance peak is observed. The polarized reflectance properties of ECDBR-450 and ECDBR-650 show similar trend as those of ECDBR-550 (Figure S7, Supporting Information).

Considering the electrochromic nature of WO_3, the optical properties of ECDBRs were expected to be tailored reversibly by applying a bias voltage. These ECDBRs were putt in 1 M $LiClO_4$ in propylene carbonate (PC) solution to study their electrochromic properties. The corresponding electrochemical reaction equation is as follows

$$WO_3 + xLi^+ + xe^- \leftrightarrow Li_xWO_3 \quad (4)$$

We can see that all three ECDBRs show clear and unique color changes under electrical stimulus, but their ribbons are different from each other (**Figure 3**). For example, at the potential of −1.1 V (vs Ag/AgCl), the color of ECDBR-450 switched from royal blue to light slate blue, while the ECDBR-550 and ECDBR-650 changed to green and orange at the same condition, respectively. In contrast, dense WO_3 film without periodic structure did not show any obvious reflection color. As for the perspective effect, all four films reveal a similar dark blue color in the full colored state (−1.1 V), but multiple colors in other states (Figures S8 and S9, Supporting Information). These results suggest that the electrically tuned optical performances of ECDBRs could be attributed to the combined effects of unique structural coloration and electrochromism.

The real-time reflectance spectra of these samples under varying driving voltage are shown in **Figure 4**. For dense WO_3 film,

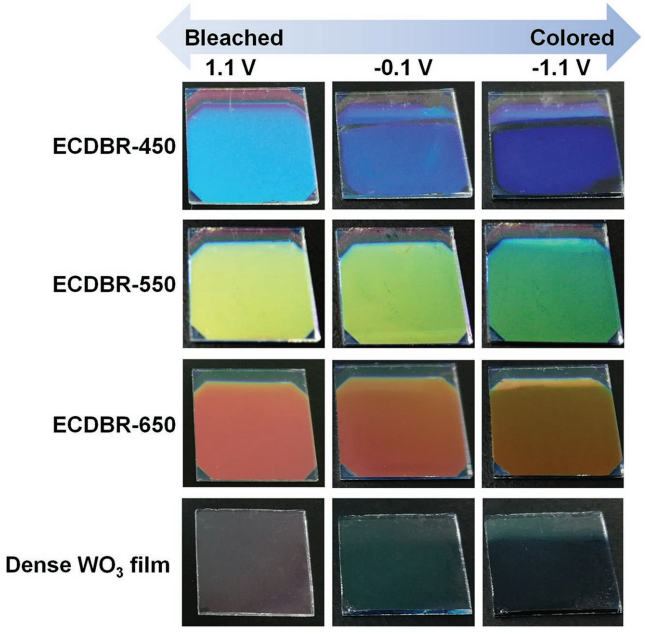

Figure 3. Electrochromic properties of dense WO_3 film and 4-bilayer ECDBRs with various Bragg wavelength (λ_B = 450, 550, and 650 nm).

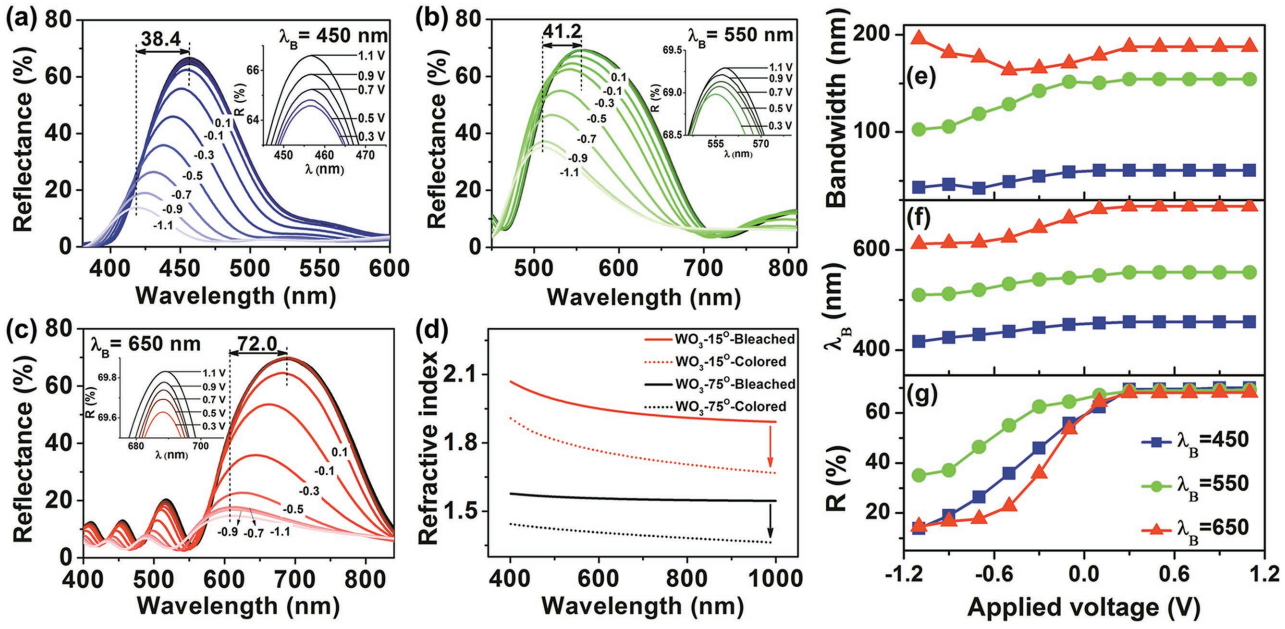

Figure 4. The dependence of reflectance spectra at normal incidence on bias voltage (vs Ag/AgCl for 30 s) for 4-bilayer ECDBRs with Bragg wavelength of a) 450 nm, b) 550 nm, and c) 650 nm, and d) the refractive indices of WO_3-15° and WO_3-75° film in colored and bleached state. The e) bandwidth, f) Bragg wavelength, and g) maximum reflectance of 4-bilayer ECDBR-450, ECDBR-550, and ECDBR-650 as a function of applied voltage.

the difference in reflectivity between the colored and bleached states is very small (Figure S10, Supporting Information). In contrast, a great dependence of reflection spectra on driving potential was observed for the ECDBRs (Figure 4a–c). With a subsequent decrease in potential from 0 to –1.1 V (vs Ag/AgCl, for 30 s), all the ECDBRs exhibit similar trends in the changes of reflection peak, that is, the peak intensity decreases gradually together with a hypsochromic shift in the reflection peak. The maximum shifts of reflection spectra and the maximum modulations of reflection intensity upon electrical stimulus were 38.4 nm/52.7%, 41.2 nm/34.2%, and 72.0 nm/55.3% for ECDBR-450, ECDBR-550, and ECDBR-650, respectively. These phenomena could be mainly attributed to colored Li_xWO_3, which simultaneously increases the light absorption and reduces the refractive index (decreasing the optical thickness) of the film (Figure 4d), and consequently leads to the subdued reflectivity and blue shift of the stop-band. The changes of optical properties (maximum reflectance, Bragg wavelength, and bandwidth) upon applied voltage are summarized in Figure 4e–g. We noted that the changes of the stop-band and reflection were greater than that for stacked WO_3/NiO multilayer owing to larger differences in the refractive index. If an anodic potential is applied (1.1 V vs Ag/AgCl, for 30 s), the reflection spectra can revert to their original state, suggesting that this process is completely reversible. In addition, the switching speed of optical property is very fast (<10 s; Table S1, Supporting Information) on account of the porous features.

The ability to control and manipulate light flow across a wide range of wavelengths validates the potential for controllable, wavelength-sensitive optical elements for thin-film photonic integration. Herein, a state-of-the-art emission-tunable microcavity luminescent device was fabricated by embedded green emitting core–shell CdSe@ZnS QDs in one normal high reflective DBR and one tuned output ECDBR, where the normal DBR was used to simplify the model. A schematic of the formed monolithic microcavity device is shown in **Figure 5**a, where the normal DBR consists of 15-bilayer alternate SiO_2/TiO_2 and a conducting ITO (≈75 nm) layer, and the ECDBR is made of 9-layer alternate WO_3-75°/WO_3-15° film. The thickness of the embedded QDs' layer is about 152 nm, equivalent to half wavelength optical thickness of a design wavelength of 523 nm. Figure 5b shows the spontaneous emission spectra observable along the cavity axis and the relative parameters are listed in Table S2 in the Supporting Information. QDs film without cavity exhibits a green emission at 523 nm with a full width at half maximum (FWHM) of 21.3 nm. By comparison, a marked bandwidth narrowing (from 21.3 to 11.4 nm) due to the cavity resonance restriction accompanied by a great PL peak intensity enhancement (3.35 times) within the cavity resonance curve were realized in the microcavity device. The origin of these unique phenomena in the microcavity lies in the Purcell effect that changes the coupling of the intramolecular transition to the vacuum electromagnetic field, thus leading to an acceleration of the radiative transition from material.[33]

By applying a negative potential, the reflectivity of the microcavity is reduced gradually together with the hypsochromic shift of the resonated dip associated with the cavity mode on account of the coloration of ECDBR (Figure S11, Supporting Information). As a result, the emission color of QDs can be tuned by extra potential. As shown in Figure 5b–e and Table S2 in the Supporting Information, when a potential of –0.1 V was applied, the QDs within the microcavity exhibited a slightly broader (FWHM = 17.5 nm) and attenuated fluorescence in comparison with their initial state, but still stronger and narrower than the QDs without cavity. If we further reduce the potential to –0.5 V, the emission peak is shifted by 10–515.7 nm, and the FWHM

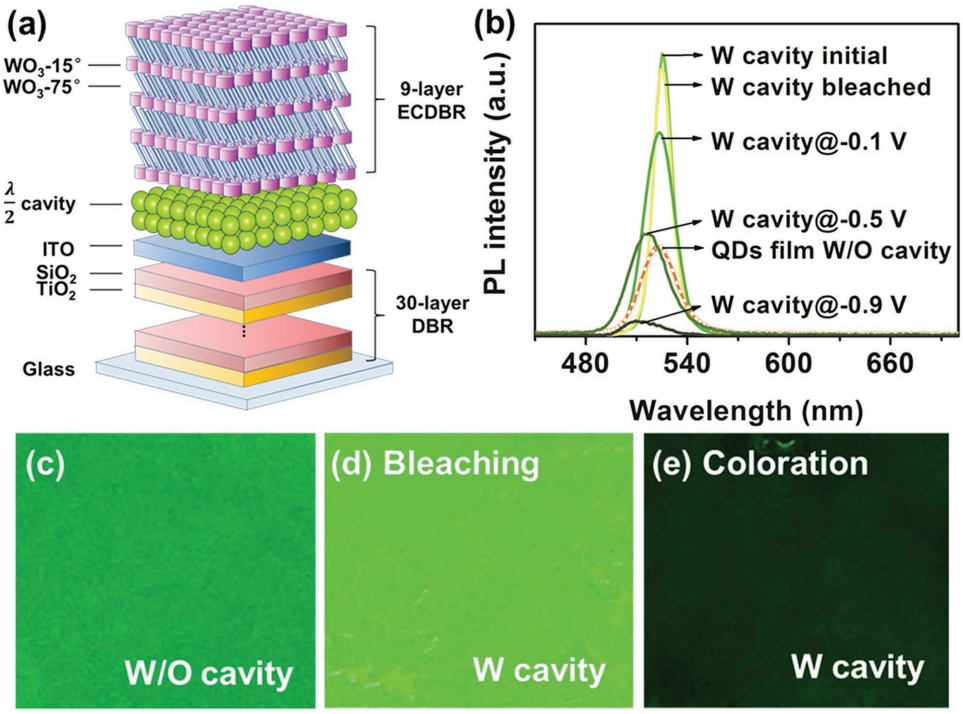

Figure 5. a) Schematic of the tunable microcavity with an embedded QDs layer. b) The PL spectra of QDs film without microcavity and that of QDs with microcavity before and after applying selected potentials of –0.1, –0.5, and –0.9 V for 120 s and irradiation with visible light (bleaching). The excitation wavelength is 355 nm. The photographs of QDs film under 355 nm light irradiation: c) without microcavity, d) with microcavity after bleaching, and e) with microcavity after coloration.

is broadened to 22.9 nm, which is even comparable to QDs without cavity. The maximum modulation (shift) of emission wavelength can reach 15.5 nm under the potential of –0.9 V accompanied by a significant decrease in emission peak intensity (decreased to less than 1/5 of reference QDs film).

To deeply understand the origin of the electrically tunable microcavity luminescence, the reflectance spectrum of microcavity was measured (Figure S11a, Supporting Information). It shows that the reflectance spectrum of the microcavity at the initial state has a wide stop-band extended from 450 to 630 nm, within which there are three cavity modes located at 472.1 (cavity mode A), 525.1 (cavity mode B), and 604.7 nm (cavity mode C), respectively. The microcavity PL emission comes from the coupling of the cavity modes to the excited states of the QD emitters, which shows a single peak at 525.8 nm in this case because the inherent narrow-band emission feature of QDs overlaps with only one of the cavity modes in the green light region (cavity mode B) (Figure 5b). The changes of microcavity PL spectra during the coloration process can be attributed to the blue shift of the cavity mode B caused by the changes of the optical constants of the top ECDBR during coloration. The reflectance spectra of the microcavity at both the initial and the colored states were simulated by transfer matrix method using the measured refractive index and calculated extinction coefficient of colored WO_3 layer (Figure S11b, Supporting Information). It shows that the simulated spectra have the similar cavity mode positions and variation trend to the experimental ones (Figure S11a, Supporting Information). The difference between the simulated and experimental spectra can be possibly attributed to the measurement error of optical constants and the thickness inhomogeneity of each layer. When the top ECDBR was colored under –0.9 V, the microcavity exhibited decreased reflectance and a broader reflective dip at 511.1 nm, which consequently caused a broad and weak PL emission. It is noted that the PL spectra can return to their initial state after bleaching, indicating a good reversibility for this spectra-tunable microcavity device. Furthermore, as a benefit of the good memory effect of electrochromic WO_3, the fluorescence spectra of this ECDBR-based luminescent device in bleached state can be stable for more than 1 month in air without persistent voltage application, and for over 5 h in colored states, which is superior to active optoelectronic devices based on liquid crystal materials that need sustained voltage to maintain the phase transition.[20] Liquid electrolyte was used in our experiments in consideration of the simple operation and convenience, whereas a polymer or a solid electrolyte is probably more promising and appropriate for practical application when considering the possibility of leakage for liquid electrolyte. Electrically tunable microcavity light-emitting diodes based on ECDBRs and solid-state electrolyte would be new practical devices worthy to develop in the future.

3. Conclusions

In summary, the periodically nanostructured WO_3 films with alternate refractive index that serve as electrically tunable ECDBRs were fabricated by a facile, one-step electron-beam

evaporation-assisted GLAD method at room temperature. Thanks to the reversible modulation of Bragg reflections from ECDBRs, the first electrically tunable microcavity luminescent device based on ECDBRs and inserted QD films were realized. The spontaneous emission from QDs film can be precisely and reversibly manipulated by varying external potential. The maximum modulation in emission wavelength, intensity, and FWHM were 15.5 nm, 317%, and 10.4 nm, respectively, at a negative voltage of only 0.9 V. The basic structure design can be further applied in electrically tunable, all-solid microcavity luminescent devices, and proceeded to the development of tunable electroluminescence and lasing techniques.

4. Experimental Section

Materials: Glass/ITO (sheet resistance 10 Ω $\square^{-1}$) substrates were obtained from Shenzhen CSG PV Energy Co., Ltd., Tungsten oxide (WO_3, 99.9%) was purchased from Chnos Elemental Technology Co., Ltd. Lithium perchlorate ($LiClO_4$, 98%), and PC (99.7%) was acquired from Sigma–Aldrich. The green emitting core–shell CdSe@ZnS QDs was provided by Mesolight Inc. with size 10–12 nm surfaced with oleic acid as ligand. All the chemicals were used without further purification.

Fabrication of ECDBRs and Microcavity Luminescent Devices: The nanostructured ECDBRs used in this study were fabricated by means of glancing-angle electron-beam evaporation at room temperature through alternate depositing WO_3 film at a glancing angles of 15° and 75° on glass/ITO substrate or QDs film, which was defined as the angle of vapor flux with respect to the substrate normal. Prior to the deposition, the glass/ITO substrates were ultrasonically cleaned with mixture of ether and ethanol, and finally dried under an oven lamp. The evaporation rates of WO_3 were ≈1.0 Å s^{-1} at pressures ≈2×10^{-3} Pa. Throughout the deposition, the thickness of the material deposited was monitored by a quartz crystal microbalance positioned at the center of chamber, while the source material was situated at the edge of the vacuum chamber.

The microcavity device has a multilayer architecture: glass/highly reflecting DBR/QDs layer/ECDBR. The highly reflecting DBR is formed by 15-bilayer alternate SiO_2 (87.5 nm) and TiO_2 (54.6 nm) films. After that, another top ITO film (≈75 nm, ≈160 Ω $\square^{-1}$) was deposited to form a conducting layer. The SiO_2, TiO_2, and ITO films were fabricated using electron-beam deposition at a temperatures 200, 200, and 300 °C with evaporation rates of 4.2, 2.6, and 3.5 Å s^{-1}, respectively. Then, the QDs film was prepared by spin-coating a QDs solution (25 mg mL^{-1} in *n*-hexane) onto the highly reflecting DBR at a speed of 600 rpm for 60 s, subsequently annealed at 120 °C for 10 min in the atmosphere. The thickness of the QDs layer was about 152 nm. Finally, the film was transferred to electron-beam vacuum chamber for depositing top low reflective ECDBR, which was formed by a 9-layer alternate WO_3-15° (66.6 nm) and WO_3-75° (84.1 nm) layer. Each layer was deposited using the electron-beam deposition method mentioned above.

Characterization: The film thicknesses were calibrated with an Ambios XP-1 surface profiler. The morphology of ECDBRs and WO_3 single layer were characterized by scanning electron microscopy (SEM, S-4800, Hitachi, Japan) and atomic force microscope (AFM, Shimadzu SPM-9700, Shimadzu, Japan). The initial transmittance spectra of ECDBRs were evaluated by a Shimadzu UV-3101PC spectrophotometer. The sheet resistance of ITO was measured by a four-point probe instrument. To measure refractive indices of WO_3 films before and after coloration, the WO_3-15° and WO_3-75° films with the thicknesses of 500 nm were deposited on ordinary and heavily doped Si (≈200 Ω $\square^{-1}$) chips, respectively. The refractive index was measured by spectroscopic ellipsometers (J.A.Woollam Co., Inc.) and fitted with Cauchy model.

The electrochemical measurements were obtained using a standard one-compartment, three-electrode electrochemical cell attached to a CHI 920C electrochemical workstation (Shanghai Chenhua Instruments Inc., China). ECDBRs, or the microcavity device were used as the working electrode (18 mm × 18 mm), a titanium plate was used as the counter electrode (5 mm × 20 mm), and Ag/AgCl (3.5 M KCl) was used as the reference electrode. The electrolyte was a $LiClO_4$ (1 M) in PC solution, which was degassed with nitrogen for 30 min prior to each test. The transmission and reflection spectra of ECDBRs and microcavity LEDs under different potentials applied by the CHI 920C electrochemical workstation were measured by Ocean Optics QE-Pro spectrometer. The PL measurements of QDs films and microcavity devices were performed with an impulse excitation (1 ns, 50 Hz) using a 355 nm UV laser (CryLaS GmbH, Berlin), focused onto the sample using an achromatic lens. The collected PL is guided into Ocean Optics QE-Pro spectrometer via an optical fiber.

Supporting Information

Supporting Information is available from the Wiley Online Library or from the author.

Acknowledgements

This work was supported by the National Natural Science Foundation of China (51503196), the Jilin Province Science and Technology Research Projects (20160520176JH, 20160520092JH, 20150101039JC), and State Key Laboratory of Luminescence and Applications.

Conflict of Interest

The authors declare no conflict of interest.

Keywords

electrochromic materials, luminescence, microcavity, photonic crystals, stimuli-responsive

Received: July 25, 2017
Revised: September 18, 2017
Published online: December 1, 2017

[1] A. Fu, H. Gao, P. Petrov, P. Yang, *Nano Lett.* **2015**, *15*, 6909.
[2] C. I. Aguirre, E. Reguera, A. Stein, *Adv. Funct. Mater.* **2010**, *20*, 2565.
[3] X. Chen, C. Chardin, K. Makles, C. Caer, S. Chua, R. Braive, I. Robert-Philip, T. Briant, P.-F. Cohadon, A. Heidmann, T. Jacqmin, S. Deleglise, *Light: Sci. Appl.* **2017**, *6*, e16190.
[4] F. Scotognella, D. P. Puzzo, A. Monguzzi, D. S. Wiersma, D. Maschke, R. Tubino, G. A. Ozin, *Small* **2009**, *5*, 2048.
[5] J. J. Wierer, A. David, M. M. Megens, *Nat. Photonics* **2009**, *3*, 163.
[6] K. J. Vahala, *Nature* **2003**, *424*, 839.
[7] M. E. Calvo, S. Colodrero, T. C. Rojas, J. A. Anta, M. Ocaña, H. Míguez, *Adv. Funct. Mater.* **2008**, *18*, 2708.
[8] C. O. Ramírez Quiroz, C. Bronnbauer, I. Levchuk, Y. Hou, C. J. Brabec, K. Forberich, *ACS Nano* **2016**, *10*, 5104.
[9] R. Betancur, P. Romero-Gomez, A. Martinez-Otero, X. Elias, M. Maymo, J. Martorell, *Nat. Photonics* **2013**, *7*, 995.
[10] D. Ge, E. Lee, L. Yang, Y. Cho, M. Li, D. S. Gianola, S. Yang, *Adv. Mater.* **2015**, *27*, 2489.
[11] J. Ge, Y. Yin, *Angew. Chem., Int. Ed.* **2011**, *50*, 1492.
[12] L. D. Bonifacio, B. V. Lotsch, D. P. Puzzo, F. Scotognella, G. A. Ozin, *Adv. Mater.* **2009**, *21*, 1641.

[13] Y. Zhao, Z. Xie, H. Gu, C. Zhu, Z. Gu, *Chem. Soc. Rev.* **2012**, *41*, 3297.
[14] A. C. Arsenault, D. P. Puzzo, I. Manners, G. A. Ozin, *Nat. Photonics* **2007**, *1*, 468.
[15] D. P. Puzzo, A. C. Arsenault, I. Manners, G. A. Ozin, *Angew. Chem., Int. Ed.* **2009**, *48*, 943.
[16] A. C. Arsenault, H. Míguez, V. Kitaev, G. A. Ozin, I. Manners, *Adv. Mater.* **2003**, *15*, 503.
[17] K. Ueno, K. Matsubara, M. Watanabe, Y. Takeoka, *Adv. Mater.* **2007**, *19*, 2807.
[18] K. Ueno, J. Sakamoto, Y. Takeoka, M. Watanabe, *J. Mater. Chem.* **2009**, *19*, 4778.
[19] M. Humar, M. Ravnik, S. Pajk, I. Muševič, *Nat. Photonics* **2009**, *3*, 595.
[20] C. Lin, Y. Jiang, C.-a. Tao, X. Yin, Y. Lan, C. Wang, S. Wang, X. Liu, G. Li, *ACS Appl. Mater. Interfaces* **2017**, *9*, 11770.
[21] T. Kuno, Y. Matsumura, K. Nakabayashi, M. Atobe, *Angew. Chem., Int. Ed.* **2016**, *55*, 2503.
[22] E. Redel, J. Mlynarski, J. Moir, A. Jelle, C. Huai, S. Petrov, M. G. Helander, F. C. Peiris, G. von Freymann, G. A. Ozin, *Adv. Mater.* **2012**, *24*, OP265.
[23] G. Cai, J. Wang, P. S. Lee, *Acc. Chem. Res.* **2016**, *49*, 1469.
[24] W. Dong, Y. Lv, L. Xiao, Y. Fan, N. Zhang, X. Liu, *ACS Appl. Mater. Interfaces* **2016**, *8*, 33842.
[25] C. G. Granqvist, *Handbook of Inorganic Electrochromic Materials*, Elsevier, Amsterdam **1995**.
[26] Y.-M. Zhang, X. Wang, W. Zhang, W. Li, X. Fang, B. Yang, M. Li, S. X.-A. Zhang, *Light: Sci. Appl.* **2015**, *4*, e249.
[27] Y. Zhang, S.-H. Lee, A. Mascarenhas, S. K. Deb, *Appl. Phys. Lett.* **2008**, *93*, 203508.
[28] L. Xiao, Y. Lv, W. Dong, N. Zhang, X. Liu, *ACS Appl. Mater. Interfaces* **2016**, *8*, 27107.
[29] B. Baloukas, J. M. Lamarre, L. Martinu, *Sol. Energy Mater. Sol. Cells* **2011**, *95*, 807.
[30] H. A. Macleod, *Thin-Film Optical Filters*, CRC Press, Boca Raton, Florida, **2001**.
[31] G. Manfredi, P. Lova, F. Di Stasio, R. Krahne, D. Comoretto, *ACS Photonics* **2017**, *4*, 1761.
[32] L. Zheng, H. Cheng, F. Liang, S. Shu, C. K. Tsang, H. Li, S.-T. Lee, Y. Y. Li, *J. Phys. Chem. C* **2012**, *116*, 5509.
[33] J. Rarity, C. Weisbuch, *Microcavities and Photonic Bandgaps: Physics and Applications*, Vol. *324*, Springer Science & Business Media, Dordrecht, Netherlands, **2012**.